

# Modifications to PM-assisted Synchronous Reluctance Machine to Achieve Rare-Earth Free Heavy-duty Traction

M. Al-ani, A. Walker, G. Vakil, D. Gerada, C. Gerada, and K. Paciura

***Abstract***—Automotive applications require electrical machines designed for high torque density, wide speed range and low cost. NdFeB magnets can achieve the high torque density and wide speed range, however, they have a high cost. Therefore, this paper explores the capability of rare-earth-free design through a PM-assisted synchronous reluctance motor (PM-SynRel). A PM-SynRel design with NdFeB has been used in this study where the NdFeB magnets have been replaced with ferrite magnets. Then, several modifications on the rotor have been made to ensure mechanical safety. Thermal analysis has been conducted last to evaluate the temperatures in the different machine parts to avoid exceeding the required limits. Finally, a prototype has been made and tested to validate the simulation results.

***Index Terms***—Rare-earth free, ferrite, PM-assisted synchronous reluctance, automotive

## I. INTRODUCTION

CLIMATE change has pushed governments toward legislation restricting the emission of greenhouse gases with the aim of a reduction of 40% by 2030 from 1990 levels [1]. Therefore, radical changes in the automotive industry were implemented, leading to the introduction of engine electrification, hybrid electric vehicles (HEVs) and fully electric vehicles (EVs). However, to reach the 40% reduction, EVs are the end goal for the automotive industry.

Heavy duty vehicles account for 5% of the traffic but 16% of transport emissions in the UK, so the electrification of these vehicles must be achieved [2]. Work has shown the performance required could be achieved with rare earth machines [3]. However due to the size and target power density of these machines, the issues with rare earth magnets are amplified: high cost, restricted availability and thermal limits. To make heavy duty traction vehicles attractive enough to move to fully electric, rare earth free traction must be achieved.

In this paper a rare earth permanent magnet (PM) machine designed for heavy duty traction is modified into a rare earth free machine. First a brief study of the state of the art heavy duty traction machines will be presented then the specific case study will be discussed. Then the design of a machine with NdFeB magnets has been presented. This design is then adapted by replacing the magnets with Ferrite. The rotor design was then modified to reduce the mechanical stress while maintaining high electromagnetic performance. Thermal

analysis has been considered to ensure temperature safety. The final design is then prototyped and tested. Finally, the rare earth free design has been compared back to the rare earth machine, the case study targets and industry goals.

## II. LITERATURE REVIEW

In literature, electrical machines for light-duty, i.e., passenger car, automotive have been widely addressed, researched and reviewed [4-6]. However, heavy-duty automotive has received little coverage in literature [7-10].

A surface-mounted permanent magnet (SPM) machine has been analytically designed and presented in [7]. The analytical model is used to optimize the machine design. The optimization explored different pole numbers with the aim to maximize the torque and minimize the machine volume. The design process then followed by finite element analysis (FEA) for verification. Dynamic analysis was then conducted to evaluate the DC voltage influence on the machine losses.

In [8], an interior permanent magnet (IPM) machine has been designed and tested. The main focus of the work is on the thermal management, direct cooling method used and investigated through studying different flow rates and cooling circuit lengths. A prototype has been made and through testing has been conducted with focus on dynamic and thermal performance.

A switched reluctance (SR) machine has been designed in [9] with an outer rotor for in-wheel drive. The design process consisted of initial sizing conducted by analytical models and FEA for more optimum and accurate design. The work also discusses a mechanical arrangement of bars to rigidly mount the rotor into the wheel. A comparison with the conventional SR machine has been made to highlight the merits of the design.

In [10], a nine-phase induction machine for heavy-duty and off-road vehicles has been developed. The work presents a drive-machine simulation to obtain the dynamic performance aiming to reach the requirement of the heavy-duty automotive application. The envelope dimensions and performance of these machines have been summarised in Table I.

In the market, there are several electrical machine products [11-15]. A summary of these products is presented in Table II. As it can be seen, induction machines (IM) and PM machines are the only topologies used, all utilising liquid cooling. All the PM machines utilise rare-earth magnets. The average peak

power of the presented products is 175kW and highest peak power of 300kW [11].

TABLE I  
DIFFERENT RESEARCH WORK ELECTRICAL MACHINES FOR HEAVY-DUTY  
AUTOMOTIVE APPLICATION

	SPM [10]	IPM [11]	SR [12]
Outer Diameter (mm)	406.445	470	360
Axial length (mm)	300.217	200	180
Airgap (mm)	1.637	-	0.9
Rated speed (rpm)	4200	1500	2000
Rated torque (Nm)	165	1300	120
Rated power (kW)	72.5	205	24
Peak torque (Nm)	325	-	200
Peak power (kW)	142	-	40

TABLE II  
MARKET AVAILABLE ELECTRIC MOTORS FOR HEAVY-DUTY TRACTION  
APPLICATION

Manufacturer	Motor Type	Peak power (kW)	Continuous power (kW)	Reference
Allison Transmission	IM	150	75	[11]
BAE	IM	200	160	[11]
Azure Dynamics	IM	97	50	[11]
Solectria	IM	78	NA	[11]
UQM Technologies	IM	200	115	[11]
Oshkosh	IM	120	[11]	
BorgWarner-Remy	PM	300	250	[12]
Volvo	PM	185	NA	[13]
Zytek continental	PM	170	125	[15]

The UK advance propulsion center (APC) has summarized the requirements for electric motors in heavy-duty automotive (trucks and buses) to meet the legislative requirements of 2025 and 2035 as shown in Table III [16]. Therefore, the near future target for electric motor design is 2kW/kg and volume power density of 6kW/l. Noting that the values in Table II are assumed at 350V, 450A with a cooling inlet temperature of 65°C. The prices are 300% mark-up on material cost and drive cycle efficiency is based on the new worldwide harmonised light vehicle test procedure (WLTP).

TABLE III  
APC FUTURE ELECTRIC MOTOR PERFORMANCE REQUIREMENTS FOR HEAVY-DUTY AUTOMOTIVE

Performance Requirements	2025	2035
Cost (\$/kW)	15	12
Continuous power density (kW/kg)	2	2.5
Continuous power density, volume (kW/l)	6	7
Drive cycle efficiency (%)	88	90

### III. DESIGN REQUIREMENTS

The aim of the design is for a heavy-duty traction application, requiring a high torque density along with a wide speed range. Fig. 1 presents the target torque-speed profile for the peak and continuous operation. Table IV lists the main target design specifications and required performance. The material specifications are HXT780T for lamination steel and NdFeB magnets grade N38UH.

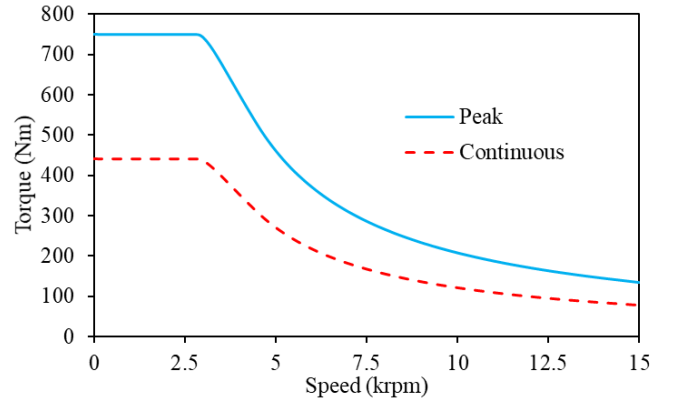


Fig. 1 Target torque-speed profile of the peak and continuous operation.

TABLE IV  
MAIN TARGET DESIGN SPECIFICATIONS AND REQUIREMENTS

Parameter	Value
Peak Power (kW)	220
Peak Time (s)	30
Peak Torque (Nm)	750
Ideal Continuous Power (kW)	150
Acceptable Continuous Power (kW)	130
Ideal Continuous Torque (Nm)	511
Acceptable Continuous Torque (Nm)	444
Base Speed (rpm)	2800
Max Speed (rpm)	15000
Max Winding Temp (°C)	180
DC Link Voltage Range (V)	620 to 760
DC Link Voltage Rated (V)	660
Mass (kg)	140
Rated Efficiency (%)	95
WLTP Drive Cycle Efficiency (%)	90

### IV. TOPOLOGY SELECTION

The latest trend in electrical machines for light-duty automotive applications have shown a significant domination of PM machines [17]. SPM machines have been used in automotive products such as Honda [18]. However, the lack of reluctance torque and limited field weakening capability made the torque-speed capability very low compared to its counterpart machines with buried magnets [19]. Both the conventional IPM with V-shaped magnet poles and permanent magnet assisted synchronous reluctance (PM-SynRel) machines have become very popular in automotive applications [17]. However, recent studies comparing both machines have shown the PM-SynRel having better or similar torque compared to that of IPM with V-shaped magnets with PM-SynRel requiring lower magnet mass and a wider speed range [20-23]. This is due to the magnetic circuit of the PM-SynRel rotor which offers higher saliency ratio [24]. Furthermore, different slot/pole combinations of PM-SynRel have been compared [24]. For high torque requirement, low number of rotor poles leads to the need of high current or number of turns. However, if the pole number is too large, a high electrical frequency is required which increases losses and requires more advanced power electronics [24-25]. Therefore, pole number of 8, 10 and 12 are more suitable for high torque wide speed range applications. As a result, the possible slot/pole combination for these pole numbers with high winding factor have been

compared in Table V. The 30/10 combination offers the highest torque and relatively low magnet mass compared to the other combinations. Therefore, 30/10 combination has been selected for this project.

TABLE V  
COMPARISON OF DIFFERENT SLOT/POLE COMBINATIONS OF PM-SYNREL MACHINE

Slot/pole	24/8	30/10	36/12
Torque (Nm)	800	845	805
Magnet weight (kg)	8	8	8
Total weight (kg)	107.8	103.8	103.2

## V. RARE-EARTH DESIGN

### A. Optimization

Initially, the 30/10 stator/rotor slot/pole combination PM-SynRel has been sized to reach the target performance presented in Section III, using a lumped parameter circuit (LPC). A global optimization has then been conducted using finite element analysis (FEA) to further improve the performance of the machine [26]. A genetic algorithm was used to optimise the machine, this is since it has the advantages of wider solution space and easier to discover global optimum compared to other optimization algorithms. This used a single objective of minimising the PM mass, as reduction of rare earth PMs was a critical goal of the machine design. However, the optimization had constraints on the minimum peak power, efficiency and maximum mass and torque ripple, as shown in table VI. Any design which did not meet these constraints was deemed unfeasible and removed from the genetic pool. Table VI presents the optimization parameters including design constrains, optimization objective/targets and the ranges of the optimized parameters. Table VII presents the optimized parameters. The electromagnetically optimized machine is the initial design. Fig. 2 presents the cross-section of the initial design.

TABLE VI  
OPTIMIZATION PARAMETERS

Parameter	Value
Constrains	
Outer diameter (mm)	300
Axial length (mm)	315
Airgap length (mm)	1.8
Degrees of freedom	
Split ratio	0.4-0.9
Slot height percentage	20-80
1st layer magnet fill percentage	0-100
2nd layer magnet fill percentage	0-100
3rd layer magnet fill percentage	0-100
Number of turns per coil	3-15
Number of parallel paths	1, 5, and 10
Objectives	
Peak power (kW)	$\geq 250$
Efficiency	$\geq 94$
PM mass (kg)	$\leq 10$
Machine mass (kg)	$\leq 140$
Torque ripple	$\leq 10$

TABLE VII  
LIST OF OPTIMIZED PARAMETERS

	Optimized
Split ratio	0.82
Slot height (mm)	16
Back-iron thickness (mm)	8.8
Magnet mass (kg)	8.4
Number of turns per coil	14
Number of parallel paths	5

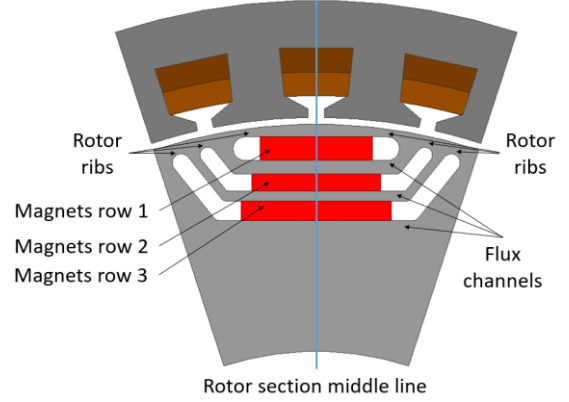


Fig. 2 Electromagnetically optimized design, initial design.

### B. Electromagnetic results

The electromagnetic performance of the initial design is presented in Table VIII. This iteration targeted a performance safety factor, i.e. providing higher performance than the requirement, to compensate for the expected performance drop due to modifications to the rotor for mechanical safety. Fig. 3 presents the torque-speed and power-speed curves of the peak and continuous operation of the initial design. It is worth noting the rotor of the optimized design has been skewed by 5 steps of 2.4 degree to reduce the torque ripple.

TABLE VIII  
PERFORMANCE OF THE INITIAL DESIGN

Parameter	Value
Peak Power (kW)	262.9
Peak Torque (Nm)	895.9
Continuous Power (kW)	215.7
Continuous Torque (Nm)	589.3
Torque ripple (%)	5.3
Base Speed (rpm)	2800
Max Speed (rpm)	15000

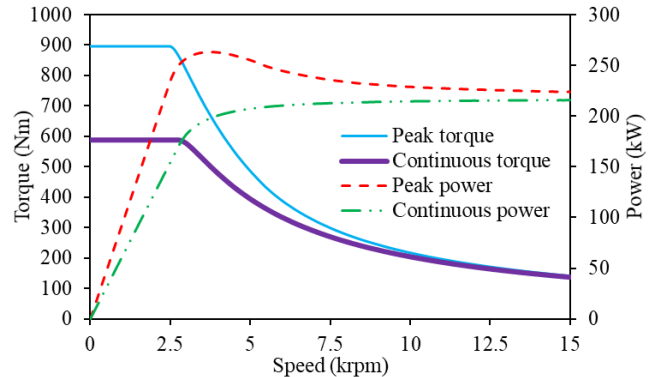


Fig. 3 Torque-speed and power-speed curves of the peak and continuous operation of the initial design.

### C. Mechanical design

Using structural FEA, the rotor of the initial design has been studied and redesigned, through several design interactions and improvements this results in mechanically safe design. The rotation speed in this analysis is set to 10% above the maximum speed, i.e. 16.5krpm, to provide a safety factor. The properties of the rotor electrical steel and magnets are shown in Table IX. The maximum allowed stress is set to 720MPa, adding a further 10% safety factor.

TABLE IX  
COMPARISON OF THE INITIAL AND OPTIMIZED PARAMETERS

Parameter	HXT780T	N38UH
Mass density (kg/m <sup>3</sup> )	7650	7500
Young's modulus (MPa)	200	160
Poisson's ratio	0.3	0.3
Yield strength (MPa)	800	60

Fig. 4 presents the stress, deformation distribution and illustration of the deformation in the rotor at 16.5krpm. The mass of the magnets causes significant deformation to the flux channels. Thus, this deformation concentrates a high stress on the outer rib, far beyond the material limits. Therefore, retaining the magnets to counter the mass and consequently the deformation is needed to reduce the maximum stress.

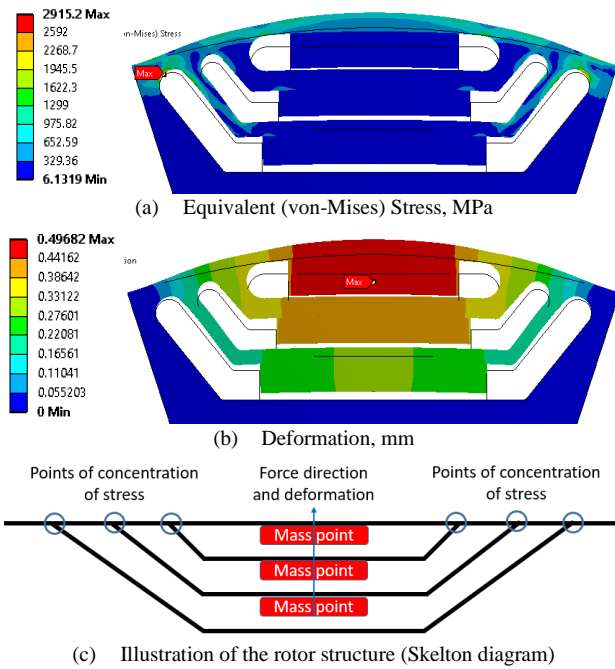


Fig. 4 Mechanical performance of the initial design rotor.

To prevent the magnets from deforming along the middle line of the rotor section, a set of 2mm thick bridges have been added at both sides of the magnets as shown in Fig. 5. The stress and deformation are shown in Fig. 5 (a) and (b), respectively. Although the maximum stress is reduced, the large deformation along the central line is still high and hence, the stress still too high. The maximum stress has moved from the outer rib to the side bridges of the third magnet row, there is also high stress in the second magnet row. The stress in the outer ribs has reduced significantly.

Therefore, the next step is segmenting the magnets into two parts separated by bridges to reduce the deformation at the middle line. The side bridges are kept to lock the magnets in their location. Sizing modifications of the rotor core dimensions have been made as shown in Fig. 6 (a). The modifications are, 1) side bridges at the second and third magnet rows increased to 3mm, 2) the outer ribs are reduced to 0.8mm, 3) the center and side bridges of the first magnet row is reduced to 0.5mm. The magnet widths are kept the same and the total length of magnets are maintained the same as the original. Fig. 6 (b) and (c) presents the stress and deformation, respectively. The maximum stress has been reduced to 668MPa which is lower than the safety limit of the material, however, the peak torque was reduced from 895.9Nm to 763.2Nm. This 17.5% torque reduction is due to the flux leakage through the bridges.

Further modifications through several iterations have been made to the rotor core to enhance the electromagnetic performance by reducing magnet leakage while maintaining the stress to the acceptable value. The final design consists of reduced outer ribs and shaped side bridges of the second and third rows to reduce magnet leakage while maintaining the stress level with a high torque of 863.7Nm. Fig. 7 presents the final design.

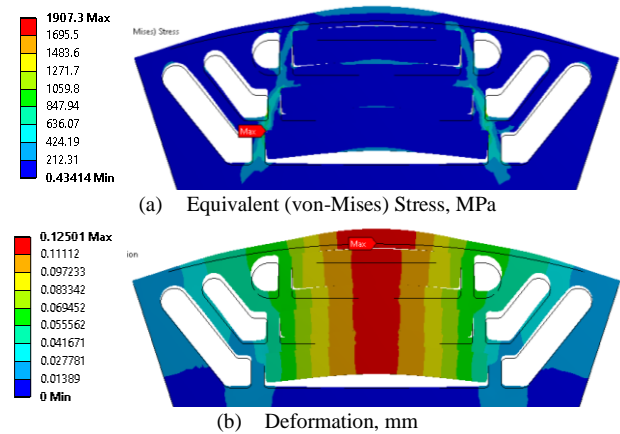
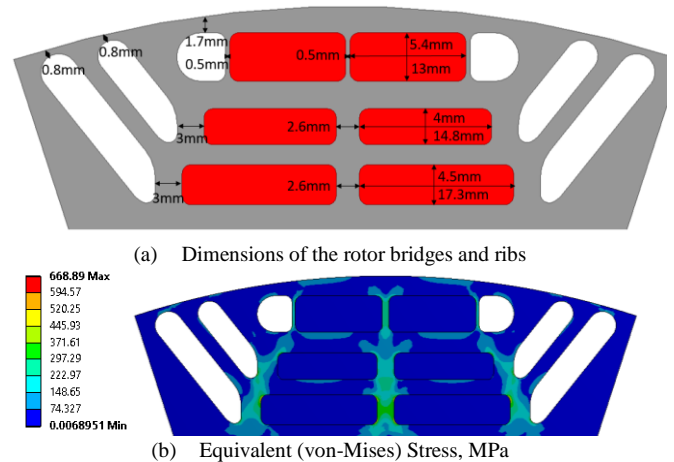


Fig. 5 Mechanical performance of the initial design rotor with side bridges.



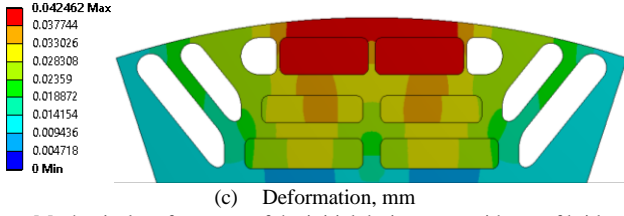


Fig. 6 Mechanical performance of the initial design rotor with net of bridges.

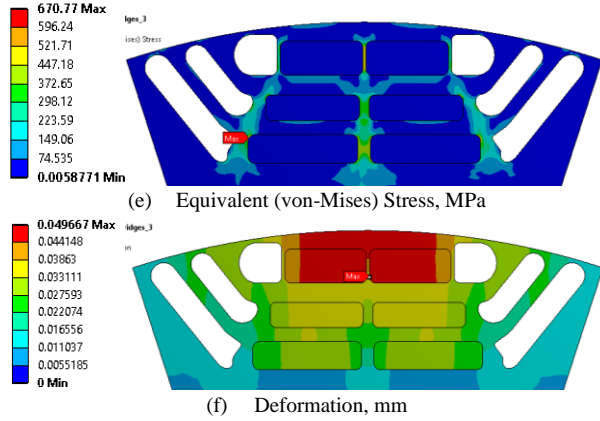
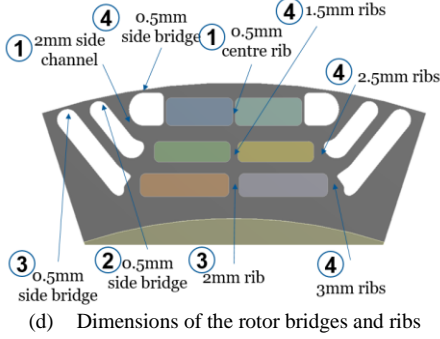


Fig. 7 Mechanical performance of the final design.

## VI. BASELINE RARE-EARTH DESIGN

Fig. 8 presents the torque-speed profile for the peak and continuous operation for the target requirement and the rare-earth design. Table X presents the design requirements of the target and the values of the rare-earth design. This original design met all the requirements but due to the heavy use of rare earth magnets.

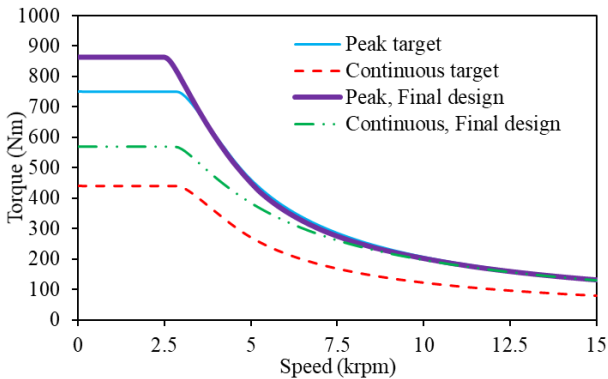


Fig. 8 Torque-speed curves of the rare-earth design.

TABLE X  
MAIN DESIGN REQUIREMENTS AND RARE-EARTH (RE) DESIGN PERFORMANCE

Parameter	Target	RE
Peak Power (kW)	220	251
Peak Torque (Nm)	750	863
Continuous Power (kW)	130	207
Continuous Torque (Nm)	444	570
Base Speed (rpm)	2800	2800
Max Speed (rpm)	15000	15000
Max Winding Temperature (°C)	180	175
DC Link Voltage Rated (V)	660	600
Peak Current (A)	NS	660
Continuous Current (A)	NS	440
Mass (kg)	140	120.5
Rated Efficiency (%)	95	96
WLTP Drive Cycle Efficiency (%)	90	93.6

## VII. RARE-EARTH FREE DESIGN

Rare-earth-free electrical machines are very desirable for automotive applications due to the cost reduction and more consistent availability of supply chain of materials. However, the key challenges for the rare-earth-free design is the expected torque and power density reduction. Therefore, in this section, the rotor is replaced by a newly designed rotor with rare-earth-free magnets, i.e. ferrite, whilst keeping the stator design consistent with the rare earth machine. This will maintain the overall volume and result in a similar mass. Hence the study will examine the performance reduction when rare-earth-free design is compared to its counterpart the rare-earth for a fixed stator design and machine volume.

### A. Initial design

Fig. 9 presents the electromagnetically designed rare-earth machine shown in Section V-B. At this stage, the machine design process has been split into two paths. The first is the rare-earth design which went through mechanical analysis and modifications as shown in Section IV. The second path is the rare-earth-free design, this design has been made using the same stator, the magnets in the rotor have been replaced with ferrite and new set of magnets have been added to the side as shown in Fig. 10. In addition to these changes the airgap has been reduced from 1.8mm to 1mm. Table XI presents the design parameters of the rare-earth-free machine. Fig. 10 presents the layout of the initial rare-earth-free rotor.

TABLE XI  
DESIGN PARAMETERS OF THE RARE-EARTH-FREE MACHINE

Parameter	Value
Outer diameter (mm)	300
Axial length (mm)	315
Airgap length (mm)	1
Split ratio	0.82
Slot height (mm)	16
Back-iron thickness (mm)	8.8
Number of turns per coil	14
Number of parallel paths	5

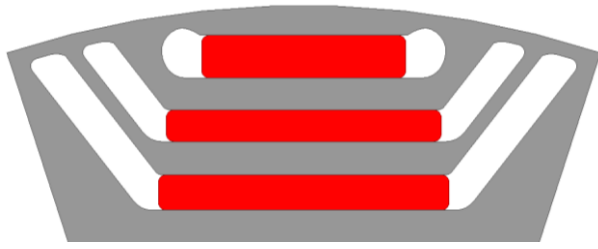


Fig. 9 Cross-section of the rare-earth rotor.

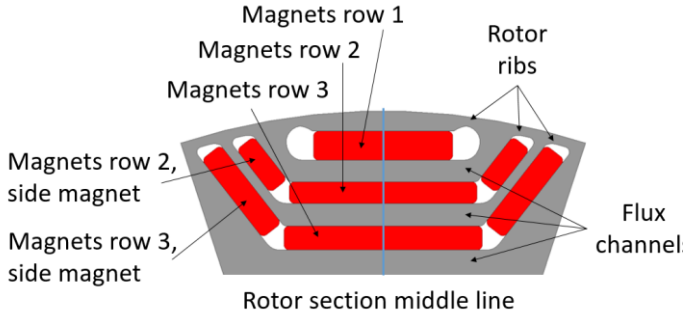


Fig. 10 The layout of the rare-earth-free rotor.

**B. Mechanical analysis**

The rare-earth-free rotor has been mechanically analysed using finite element analysis (FEA). A rotation speed of 16.5krpm has been targeted for the safety limit, 10% over maximum operating speed. The rotor core material has a yield strength of 800MPa, therefore, a limit of 720MPa has been used allowing for another 10% safety factor. Fig. 11 presents the stress and deformation of the initial rotor. Similar, to the process of designing the rare-earth machine, a rotor modification is required.

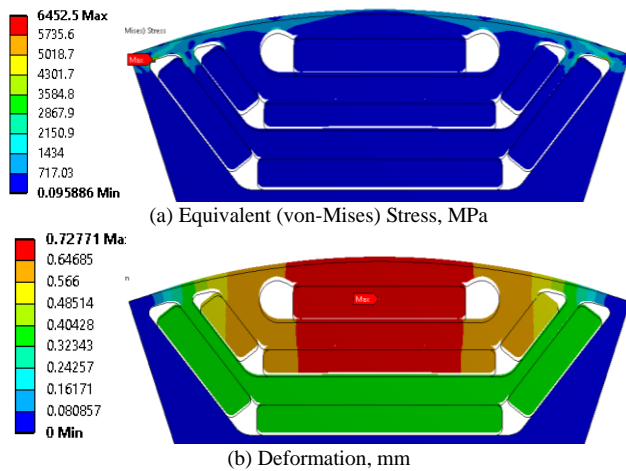


Fig. 11 Stress and deformation of the rare-earth-free rotor.

The net of bridges technique has been employed to the initial rotor. Fig. 12 presents the rotor layout of the modified design with the net of bridges. It can be seen that the centre magnets have been segmented into two and separated with bridges, hence the total length of these magnets has been reduced to allow space for the bridges. The side magnets length has been increased while the outer ribs thicknesses have been reduced to 0.5mm. The side magnet thickness has been increased slightly

to allow it to be partially buried in the rotor core. These modifications allow for high retention of the magnets and hence reduces deformation and the consequent stress while maintaining good electromagnetic performance by minimizing the magnet flux leakage paths. Fig. 13 presents the stress and deformation of the rotor with the net of bridges. It can be seen that the stress level has been reduced to 655MPa, below the material limit of 720MPa.

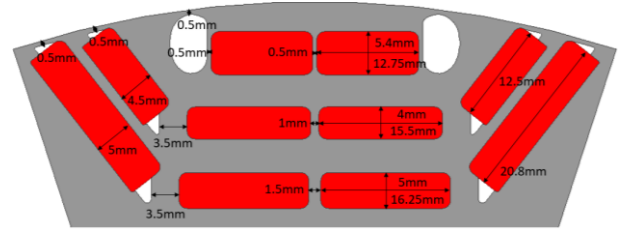


Fig. 12 Modification applied on the rotor core to reduce mechanical stress.

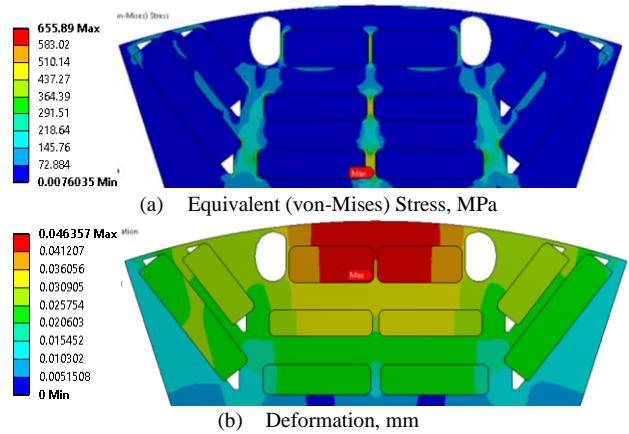


Fig. 13 Mechanical performance of the design rotor with net of bridges.

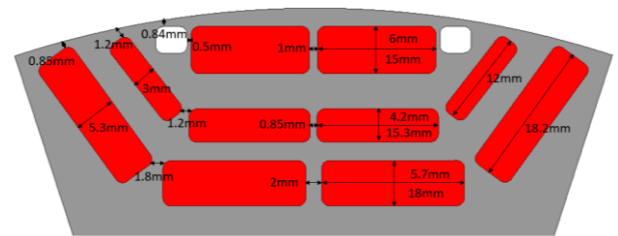


Fig. 14 Modification applied on the rotor core to enclose the magnets.

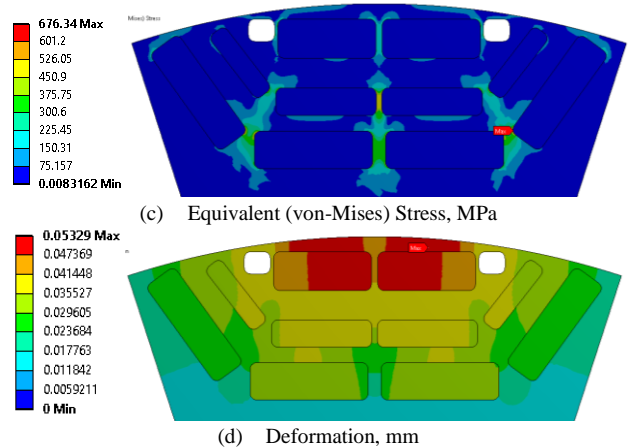


Fig. 15 Mechanical performance of the design rotor with enclosed magnets.

However, to ensure the mechanical safety of the magnets, a solution of fully enclosed magnets by the rotor core has been employed. This adds extra mechanical safety for the magnets, the enclosure of the magnets by the rotor core and endcaps ensures that even if the magnets are damaged, they would be held in place. Fig. 14 presents the rotor modification with fully enclosed magnets. The modifications consist of: the centre magnets are moved toward the surface; the side magnet thicknesses are reduced and the length of the centre magnets at the first and third row increased. These changes allow for less mechanical stress and enhance the torque. Fig. 15 presents the stress and deformation of the final design, this shows the minimization of the bridges and ribs while maintaining an acceptable mechanical stress level, i.e. lower than the stress limit of the material.

### VIII. THERMAL ANALYSIS

The temperature rise in the machine has been evaluated using a thermal LPC with losses from FEA. A cooling jacket with a 9.6L/min flow rate, 65°C inlet temperature and cooling liquid of ethylene glycol-based water solution (EGW50/50) has been used. Two conditions have been evaluated 1) The temperature at continuous load condition, steady-state and 2) The temperature at a duty cycle of 30-second peak condition, i.e. maximum losses at peak operation. Table XII lists the temperature in the different machine parts. It can be seen the maximum winding temperature is 177°C which is lower than the target maximum allowed temperature of class 3 winding insulation of 180°C. The magnet temperature is 72°C which is significantly lower than the Ferrite limit of 200°C.

TABLE XII  
TEMPERATURE OF DIFFERENT MACHINE PARTS OF THE RARE-EARTH-FREE DESIGN

Machine part	Temperature (°C),	
	Continuous	Peak
Winding average	125	142
Winding maximum	152	177
Stator tooth	90	93
Stator yoke	86	89
Rotor pole	71	72
Magnet	71	72

### IX. RARE-EARTH FREE MACHINE PERFORMANCE

Fig. 16 presents the torque waveform of the rare-earth-free design. It can be seen that the torque ripple is relatively low, i.e. 7%, due to the use of rotor skewing of 5 steps of 1.6 degrees.

A comparison has been made between the fully multi-physics designed rare-earth machines. Fig. 17 presents the cross-section of both machine rotors. The stator and required operation conditions are identical in both machines.

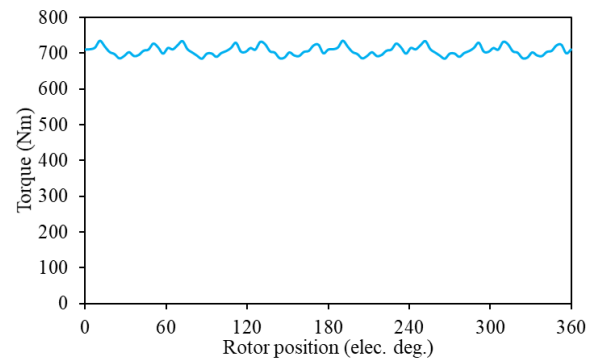


Fig. 16 Electromagnetic torque.

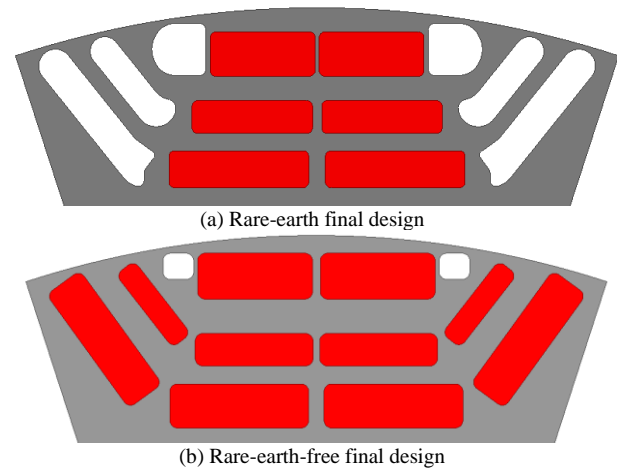
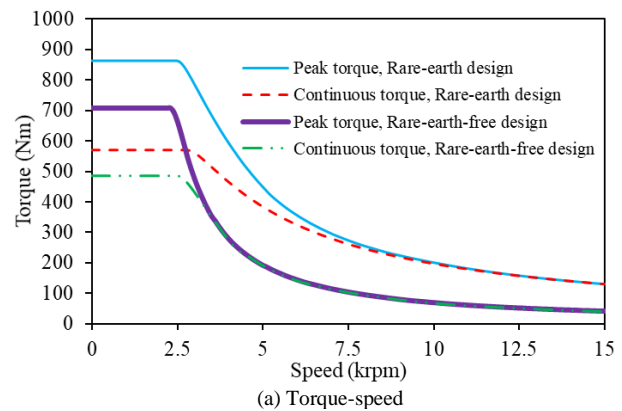


Fig. 17 Cross-section of the rare-earth and rare-earth-free machines

The torque-speed curves are compared in Fig. 18. It can be seen that rare-earth-free design has less torque at the constant torque region in both continuous and peak conditions. Similarly, the maximum power of the rare-earth-free design is lower in both conditions.



(a) Torque-speed

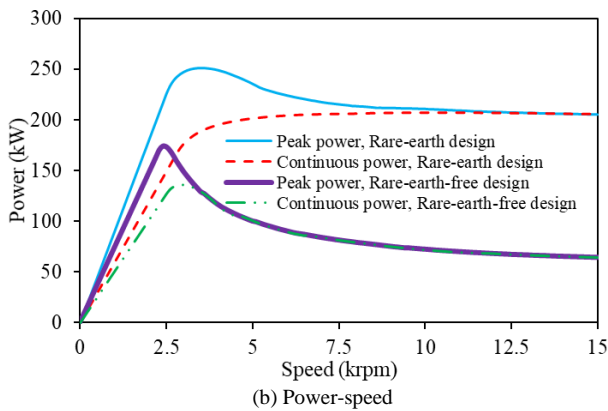


Fig. 18 Torque-speed and power-speed characteristics of the rare-earth and rare-earth-free machines.

Fig. 19 presents the efficiency map of the rare-earth and rare-earth-free machines. The maximum efficiency of the rare-earth-free is located at higher speed region, i.e. 8000rpm to 15000rpm. Whereas, the rare-earth design has the high efficiency at lower speeds, i.e. <8000rpm. This suggests the rare-earth-free machine in heavy-duty tractions requires higher power input/higher power consumption during vehicle acceleration and take off.

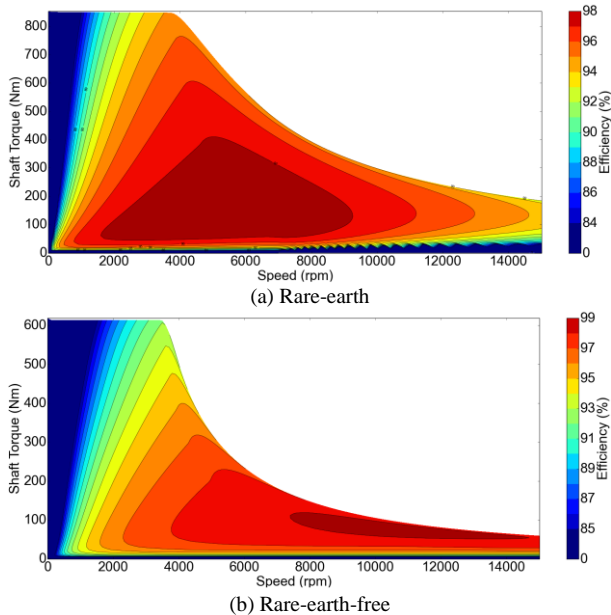


Fig. 19 Efficiency of the rare-earth and rare-earth-free machines.

Fig. 20 presents a comparison between the rare-earth-free design and the design target. It can be seen that the rare-earth-free design achieved the required torque at continuous operation condition and slightly lower torque at peak condition. However, the maximum power in both operation conditions is lower than the target and continues to be below at higher speeds. This is due to the field weakening factor of the rare-earth-free design being 4. To achieve the highest torque-speed characteristics possible a field weakening factor of 1 need to be reached. In the rare-earth-free design, the weak ferrites are prone to field weakening at a higher rate than the NdFeB magnets. Table XIII presents the performance of the rare-earth

(RE) design, rare-earth-free (REF) design and the design target.

As can be seen, the rare-earth-free machine can achieve the required torque and power at continuous condition, while at peak condition, 93% of the torque and 68% of the power are achieved. Therefore, the rare-earth-free machine can achieve the required torque but it lacks in achieving the power.

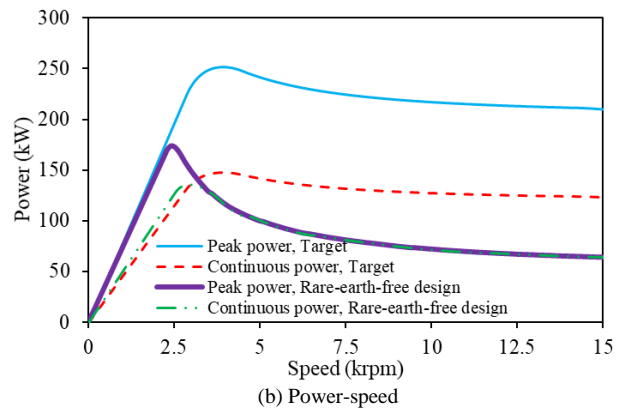
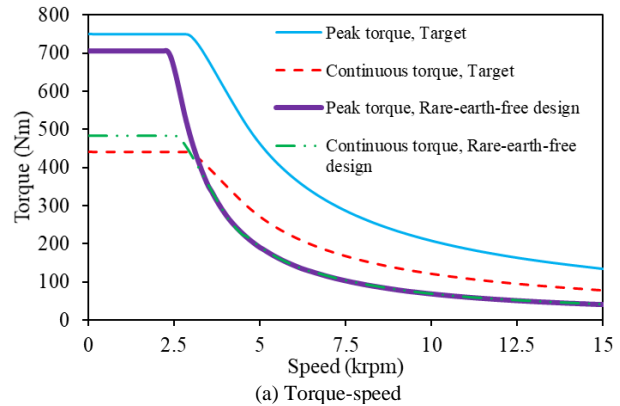


Fig. 20 Comparison of the torque-speed characteristics of the rare-earth-free machine with the design target.

TABLE XIII  
MAIN DESIGN REQUIREMENTS AND RARE-EARTH (RE) AND RARE-EARTH FREE (REF) DESIGNS PERFORMANCE

Parameter	Target	RE	REF
Peak Torque (Nm)	750	863.7	706
Peak Power (kW)	220	251.5	173
Active Target Mass (kg)	140	120.5	127
Complete Machine Mass (kg)	160	150	157.5
Active Peak Power Density (kW/kg)	NS	2.08	1.36
Active Peak Power Density (kW/l)	NS	10.75	7.7
Peak Power Density (kW/kg)	NS	1.67	1.1
Peak Power Density (kW/l)	NS	3.8	2.6
Continuous Torque (Nm)	444	570.5	484
Continuous Power (kW)	130	207.3	135
Active Continuous Power Density(kW/kg)	NS	1.72	1.06
Active Continuous Power Density (kW/l)	NS	8.8	6
Continuous Power Density (kW/kg)	NS	1.3	0.86
Continuous Power Density (kW/l)	NS	3.1	2
Base Speed (rpm)	2800	2800	2600
Max Speed (rpm)	15000	15000	15000
Target Rated Efficiency (%)	95	97	98
Target WLTP Drive cycle Efficiency (%)	90	93.6	91.1
Max Winding Temp (°C)	180	176	177
DC Link Voltage Rated (V)	660	600	600
Peak Current (A)	660	660	660
Continuous Current (A)	440	440	440

By examining the torque-speed and power-speed curves of the rare-earth-free machine, it can be seen that the field weakening factor is 4. This is due to the weak ferrite magnets which results in high field weakening and the presences of the bridges around the magnets which create a path for the magnets field when d-axis current is applied. Therefore, to achieve lower field weakening factor of 1, thicker magnets and reduced bridges are preferred.

## X. EXPERIMENTAL VALIDATION

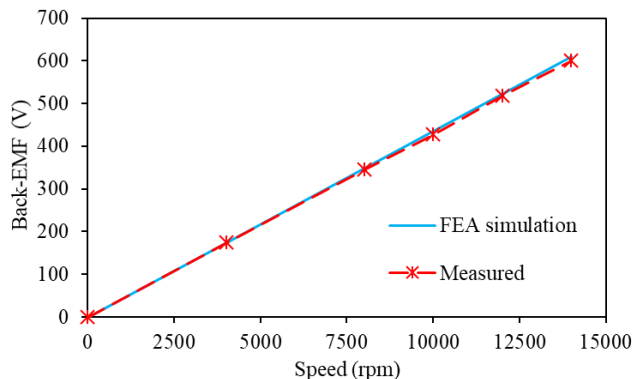
A prototype of the machine has been constructed shown in Fig. 21. Spin and load tests have been conducted and compared with simulation predicted results.



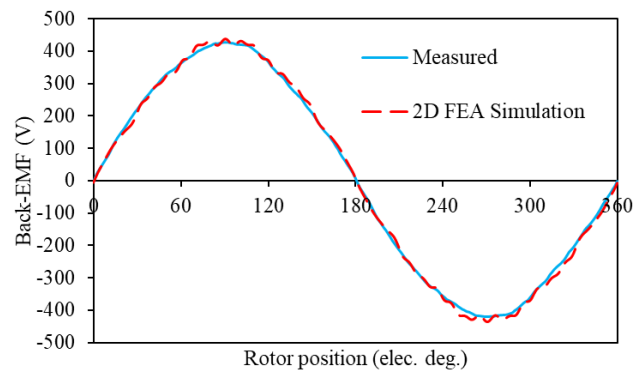
Fig. 21 Prototype of rare-earth-free machine.

### A. Spin test

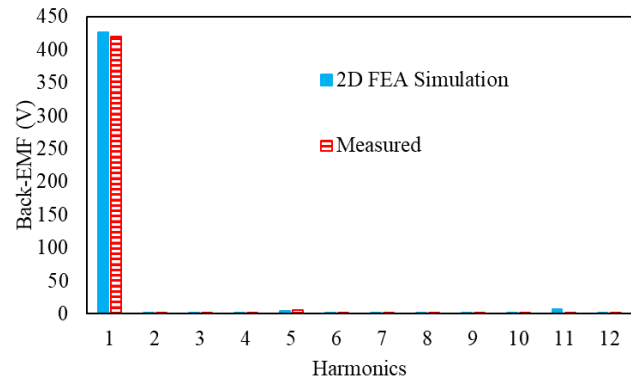
First, the spin test has been conducted to evaluate the mechanical stability of the machine and the winding connections. The machine is mounted onto a test rig and the shaft is connected to the test rig dyno. The machine phases are connected to an oscilloscope to measure the back-EMF. The machine was then spun up to 14krpm at intervals of 1000rpm while recording the back-EMF and monitoring thermal and vibration conditions. Fig. 22 presents the measured and FEA predicted back-EMF across the speed range and the waveform at 10krpm.



(a) Back-EMF (peak) versus speed



(b) Back-EMF waveform at 833.33Hz.



(c) Back-EMF harmonics at 833.33Hz.

Fig. 22 Spin test back-EMF results.

### B. Load test

An initial load test has been conducted on the machine on the test rig while monitoring the vibration and temperature. The test has been conducted at low load points to ensure mechanical and electrical safety. Similarly, only q-axis current has been used to allow easier evaluation the controller and ensure the machine was operating safely. Table XIV presents a comparison between the measured points and the FEA predicted.

TABLE XIV  
MEASURED AND PREDICTED TORQUE AT DIFFERENT CURRENTS

Load points	Measured (Nm)	Predicted (Nm)
$I_q=80A, I_d=0 @ 3000rpm$	49.2	50
$I_q=80A, I_d=0 @ 4000rpm$	49.2	50
$I_q=95A, I_d=0 @ 5000rpm$	59	60
$I_q=40A, I_d=0 @ 6000rpm$	24.6	25

## XI. CONCLUSION

This paper explores the capability of designing a rare-earth-free synchronous reluctance electric machine for a heavy-duty automotive application. Previously a synchronous reluctance machine with NdFeB magnets has designed and constructed. The rare-earth-free design process started with modifying the existing machine rotor design by replacing the magnets with ferrite and decreasing the airgap from 1.8mm to 1mm while maintaining the same stator. The rotor is then mechanically analysed and modified to ensure mechanical safety. Similarly, a thermal study has been conducted to maintain the temperature rise below the allowed limit of 180°C. Then, a comparison with

the final rare-earth machine has been made to evaluate the capability of the rare-earth-free design. It is found that a rare-earth-free design can achieve the continuous constant torque requirement, however, lower values have been acquired for peak condition. Finally, a prototype of the final design is made and tested, the measured results showed an excellent agreement with the simulated counterpart.

Compared to the rare-earth machine, the rare-earth-free can achieve 70% of the peak power and 65% of the continuous power. Additionally, compared to the application targets the rare-earth-free machine achieved the continuous torque and power and 93% of the torque and 68% of the power at peak condition. Finally, the rare-earth machine achieved the volume continuous volume power density, 6kW/l, of the ATC 2025, however, the machine achieved around half the ATC 2025 target continuous mass power density 1.06kW/kg. In conclusion, as expected the performance of the rare earth free machine is below that of the rare earth machine, however it is shown that there is potential for a rare-earth-free machine to meet both the acceptable case study requirements and future requirements of the APC.

## XII. REFERENCE

- [1] [https://ec.europa.eu/clima/policies/strategies/2030\\_en](https://ec.europa.eu/clima/policies/strategies/2030_en)
- [2] [https://assets.publishing.service.gov.uk/government/uploads/system/uploads/attachment\\_data/file/984685/transport-and-environment-statistics-2021.pdf](https://assets.publishing.service.gov.uk/government/uploads/system/uploads/attachment_data/file/984685/transport-and-environment-statistics-2021.pdf)
- [3] M. Al-Ani et al., "Multi-physics Design Optimisation of PM-assisted Synchronous Reluctance Motor for Traction Application," *IECON 2019 - 45th Annual Conference of the IEEE Industrial Electronics Society*, 2019, pp. 4353-4359
- [4] B. Bilgin et al., "Making the Case for Electrified Transportation," in *IEEE Transactions on Transportation Electrification*, vol. 1, no. 1, pp. 4-17, June 2015.
- [5] M. Zeraoulia, M. E. H. Benbouzid and D. Diallo, "Electric Motor Drive Selection Issues for HEV Propulsion Systems: A Comparative Study," in *IEEE Transactions on Vehicular Technology*, vol. 55, no. 6, pp. 1756-1764, Nov. 2006.
- [6] M. Popescu, J. Goss, D. A. Staton, D. Hawkins, Y. C. Chong and A. Boglietti, "Electrical Vehicles—Practical Solutions for Power Traction Motor Systems," in *IEEE Transactions on Industry Applications*, vol. 54, no. 3, pp. 2751-2762, May-June 2018.
- [7] Z. Wu, D. Depernet, C. Kieffer, F. Dubas, D. Hissel and C. Espanet, "Electrical motor design for hybrid heavy-duty electrical powertrain," *2009 IEEE Vehicle Power and Propulsion Conference*, Dearborn, MI, 2009, pp. 486-493.
- [8] P. Lindh et al., "Performance of a Direct-Liquid-Cooled Motor in an Electric Bus Under Different Load Cycles," in *IEEE Access*, vol. 7, pp. 86897-86905, 2019.
- [9] A. Labak and N. C. Kar, "Outer rotor switched reluctance motor design for in-wheel drive of electric bus applications," *2012 XXth International Conference on Electrical Machines*, Marseille, 2012, pp. 418-423.
- [10] C. Yuan, M. S. Illindala, K. D. Ramamoorthy and O. Alkhouli, "Nine-phase induction machine with electric pole change for emerging heavy-duty and off-road micro/mild hybrid vehicle applications," *2017 IEEE Industry Applications Society Annual Meeting*, Cincinnati, OH, 2017, pp. 1-8.
- [11] A. M. El-Refaei, "Motors/generators for traction/propulsion applications: A review," in *IEEE Vehicular Technology Magazine*, vol. 8, no. 1, pp. 90-99, March 2013.
- [12] [https://cdn.borgwarner.com/docs/default-source/default-document-library/remy-pds---hvh410-150-sheet-euro-pr-3-16.pdf?sfvrsn=a642cd3c\\_11](https://cdn.borgwarner.com/docs/default-source/default-document-library/remy-pds---hvh410-150-sheet-euro-pr-3-16.pdf?sfvrsn=a642cd3c_11)
- [13] <https://www.greencarcongress.com/2018/04/20180412-volvo.html>
- [14] [https://new.abb.com/motors-generators/iec-low-voltage-motors/heavy-electric-vehicles?utm\\_campaign=e-mobility&utm\\_medium=news&utm\\_source=press-release](https://new.abb.com/motors-generators/iec-low-voltage-motors/heavy-electric-vehicles?utm_campaign=e-mobility&utm_medium=news&utm_source=press-release)
- [15] <http://www.zytekautomotive.co.uk/products/electric-engines/170kw/>
- [16] M. Al-Ani et al., "Comparative Study of Different Electrical Machines in Electric and Hybrid Vehicles," in *IEEE Transactions on vehicular technology*, in press.
- [17] [https://www.apcuk.co.uk/app/uploads/2018/02/EMC\\_Full\\_Pack.pdf](https://www.apcuk.co.uk/app/uploads/2018/02/EMC_Full_Pack.pdf)
- [18] Staunton, R.H., Burress, T.A., and Marlino, L.D. Evaluation of 2005 Honda Accord Hybrid Electric Drive System. United States: N. p., 2006. Web. doi:10.2172/891260.
- [19] P. B. Reddy, A. M. El-Refaei, K. Huh, J. K. Tangudu and T. M. Jahns, "Comparison of Interior and Surface PM Machines Equipped With Fractional-Slot Concentrated Windings for Hybrid Traction Applications," in *IEEE Transactions on Energy Conversion*, vol. 27, no. 3, pp. 593-602, Sept.
- [20] Z. Q. Zhu, W. Q. Chu and Y. Guan, "Quantitative comparison of electromagnetic performance of electrical machines for HEVs/EVs," in *CES Transactions on Electrical Machines and Systems*, vol. 1, no. 1, pp. 37-47, March 2017.
- [21] Huynh, T.A.; Hsieh, M.-F. Performance Analysis of Permanent Magnet Motors for Electric Vehicles (EV) Traction Considering Driving Cycles. *Energies* 2018, *11*, 1385.
- [22] A. Walker, M. Galea, C. Gerada, A. Mebarki and D. Gerada, "A topology selection consideration of electrical machines for traction applications: towards the FreedomCar 2020 targets," *2015 Tenth International Conference on Ecological Vehicles and Renewable Energies (EVER)*, Monte Carlo, 2015, pp. 1-10.
- [23] A. Walker, M. Galea, D. Gerada, C. Gerada, A. Mebarki and N. Brown, "Development and design of a high performance traction machine for the FreedomCar 2020 traction machine targets," *2016 XXII International Conference on Electrical Machines (ICEM)*, Lausanne, 2016, pp. 1611-1617.
- [24] W. Wu, X. Zhu, L. Quan, Y. Hua, and Q. Lu, "Comparative Study of IPM Synchronous Machines with Different Saliency Ratios Considering EVs Operating Conditions," *Progress In Electromagnetics Research M*, Vol. 71, 19-29, 2018.
- [25] A. Walker, M. Galea, C. Gerada, A. Mebarki and D. Gerada, "Design considerations for high performance traction machines: Aiming for the FreedomCar 2020 targets," *2015 International Conference on Electrical Systems for Aircraft, Railway, Ship Propulsion and Road Vehicles (ESARS)*, Aachen, 2015, pp. 1-6.
- [26] M. Al-Ani et al., "Multi-physics Design Optimisation of PM-assisted Synchronous Reluctance Motor for Traction Application," *IECON 2019 - 45th Annual Conference of the IEEE Industrial Electronics Society*, 2019, pp. 4353-4359